Journal of Materials Chemistry A

Accepted Manuscript

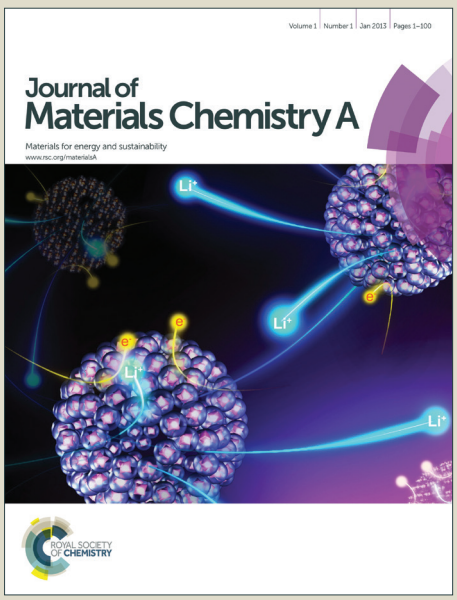

ROYAL SOCIETY OF CHEMISTRY

www.rsc.org/materialsA

Journal Name

RSCPublishing

COMMUNICATION

Flexible Free-Standing Hydrogen-treated Titanium Dioxide Nanowire Arrays as High Performance Anode for Lithium Ion Batteries

Cite this: DOI: 10.1039/x0xx00000x

Received 00th January 2012,
Accepted 00th January 2012

DOI: 10.1039/x0xx00000x

www.rsc.org/

Yi Liu,* Chunjie Liu, and Jianle Li

Herein, we fabricate flexible free-standing TiO_2 nanowire arrays and create Ti^{3+} (oxygen vacancy) via hydrogenation to improve the electrical conductivity. The hydrogenated-TiO_2 nanowires deliver a high reversible capacity of 517 mAh g^{-1} at a current density of 1 C. Moreover, the hydrogenated-TiO_2 nanowires have an excellent rate performance as they still retain 70 mAh g^{-1} when the current density increases to 50 C. The electrochemical performance of the hydrogenated-TiO_2 nanowires is due to the improved conductivity of TiO_2 nanowires arising from the formation of Ti^{3+} (oxygen vacancy) via hydrogenation.

Among the various transition metal oxides available for use as the active anode material, titanium dioxide (TiO_2) has been widely considered as one of the promising anode materials in LIBs due to its attractive properties, such as environmental friendliness, low cost, high Li-insertion potential (1.6–1.8 V vs Li^+/Li), low volume expansion and long cycle life when compared to commercialized carbon (graphite) anode materials. [1-3] However, the main disadvantage of TiO_2 is its poor electronic conductivity, resulting in poor rate capability of the cells. [4] One of the most promising strategies is to develop nanostructured TiO_2 electrodes. [5] For instance, various TiO_2 nanostructures such as nanotubes [6], nanowires [7], nanosheets [5], nanoparticles [8], nanospindles [9] have been synthesized and showed attractive electrochemical performance in LIBs. Another strategy to improve the rate capability of TiO_2 is combining it with highly conductive carbon materials. [3, 10-12] Yang *et al*. reported a kind of TiO_2@C composite nanowires that could achieve a discharge capacity of 200 mAh g^{-1} at a current density of 2.2 C. [13] TiO_2-carbon nanofiber composite was recently fabricated and reported to be able to deliver100 mAh g^{-1} at 3.7 C. [14] Despite these achievements, the rate performance of TiO_2 anode at high current density (especially up to 30 C) is still not satisfied. Therefore, it is still desirable to improve the rate performance of TiO_2 anode.

In recent years, flexible LIBs have attracted increasing attention because of their great potential applications in roll-up displays, photovoltaic cells, and wearable electronic devices. The essential component to the fabrication of flexible LIBs is to develop flexible high-performance electrodes. [15-17] To the best of our knowledge, there are few reports on the flexible TiO_2 based anodes. [16, 18, 19] In this work, we describe a facile route to fabricatehydrogenated-TiO_2 nanowire arrays via hydrothermal growth and hydrogenation. Oxygen vacancy has proven to significantly improve the electrochemical properties of the metal oxides. [20-24] For instance, the catalytic activity and capacitive performance of MnO_2 can be enhanced by generating oxygen deficiency during hydrogenation process. [20, 21] The hydrogenated Pt/$CaMnO_3$ hybrid exhibits an enhanced conductivity due to the introduction of the oxygen vacancy. [22] For TiO_2, hydrogenation was employed to create Ti^{3+} sites that associate with oxygen vacancies, [25] which could significantly enhance the electronic conductivity of TiO_2 and thereby enhance the performance of TiO_2 in supercapacitors [26, 27], water splitting [28, 29], photocatalysts [30] and so on. We choose to anneal the TiO_2 nanowires in hydrogen gas atmosphere because hydrogen it is a reducing gas with very light weight that may facilitate easy diffusion and movement of ions in the TiO_2. [28, 31] Free-standing hydrogenated-TiO_2 nanowire arrays grown on flexible carbon fiber not only provide more reaction sites for Li ions insertion/deinsertion, but also provide good mechanical support and serve as a binder-free electrode. Such features make the hydrogenated-TiO_2 nanowires possess enhanced capacity and stability as well as rate capability. The hydrogenated-TiO_2 nanowires deliver a high capacity of 517 mAh g^{-1} at 1 C and excellent cyclic stability with 83% retention of its initial capacity at 10 C after 500 cycles. More importantly, the hydrogenated-TiO_2 nanowires exhibit attractive rate capability that could retain a relatively higher capacity of 70 mAh g^{-1} at 50 C. Such excellent electrochemical performance confirms the hydrogenated-TiO_2 nanowire arrays as effective anode material for high performance LIBs.

Experimental Section

Synthesis of the flexible binder-free hydrogenated-TiO_2 nanowires arrays: hydrogenated-TiO_2 nanowires arrays were synthesized by one-step hydrothermal method and post-annealing. TiO_2 nanowires were firstly grown on carbon fiber by a seed-assisted hydrothermal method reported elsewhere with slight modification. [17] The clean carbon fiber were immersed into 0.2 M $TiCl_4$ aqueous solution for

10 min and heated on a hotplate in air at 350 °C for 10 min, forming TiO_2 nanoparticles on the carbon fiber surface. 20 ml of concentrated hydrochloric acid (37%) was diluted with 20 ml deionized (DI) water, and mixed with 0.6 ml titanium n-butoxide. This clear solution mixture together with the carbon fiber coated with TiO_2 nanoparticles were transferred to a Teflon-lined stainless steel autoclave (50 ml volume). The sealed autoclave was heated in an electric oven at 160 °C for 5 hours, and then allows it cool down slowly at room temperature. The obtained sample was annealed in air (denoted as Air-TiO_2) and H_2 (denoted as 550 °C-hydrogenated TiO_2) at 550 °C for 1 hour.

Electrochemical measurements: The electrochemical tests were carried out in CR2032 coin type cells. Carbon fiber uniformly covered with hydrogenated TiO_2 nanowire arrays were cut into an area of 0.8cm x 0.8cm. Both the carbon fiber with loading samples and bare carbon fiber were weighed in a high-precision analytical balance (Sartorius, max weight 5100 mg, *d*=0.001 mg). The reading difference was the exact mass for the coated samples on carbon textile. The mass of the active materials was calculated to be 1.37 mg/cm^2. Coin cells (CR2032) were fabricated with the hydrogenated TiO_2 nanowire arrays as anode, lithium metal as the counter electrode, Celgard 2400 as the separator, and LiPF6 (1M) in ethylene carbonate/ dimethyl carbonate/diethyl carbonate (EC/DMC/DEC, 1:1:1 vol%) as the electrolyte. The cell was assembled in an Ar-filled glove box. The rate capability and cycle life of the cells were tested in a potential window of 0.01–3V (vs.Li^+/Li) by a battery testing system (Neware CT3008-164, Shenzhen, China). Cyclic voltammetry (CV) at a scan rate of 0.1 mV/s and electrochemical impedance spectroscopy (EIS) were conducted on electrochemical working station (CHI 760d, Chenhua, Shanghai) at a frequency range of 10^{-1} Hz - 10^5 Hz.

Material characterization: Scanning electron microscopy (SEM) images were collected with a field-emission SEM (Hitachi S-4800II). Transmission electron microscopy (TEM) images were collected in a FEI Monochromated F30 UT Technai TEM/STEM operated at 200 kV. X-Ray diffraction (XRD) spectra were collected with XRD, D8 ADVANCE. Diffraction spectra were recorded from a 2 Theta angle of 10 to 70° with a step size of 0.02° at a rate of 1° per min. Raman spectroscopy measurements were carried out on a Nicolet Almega XR Dispersive Raman spectrometer (laser wavelength 780 nm). X-Ray photoelectron spectroscopy (XPS) was performed on a RBD upgraded PHI-5000C ESCA system (Perkin-Elmer) using Mg-monochromatic X-ray at a power of 25 W with an X-ray-beam diameter of 10 mm, and a pass energy of 29.35 eV. The pressure of the analyzer chamber was maintained below 5 x10^{-8} Pa during the measurement.

Results and Discussion

Rutile TiO_2 nanowire arrays were first fabricated on carbon fiber substrates, using a seed mediated hydrothermal method (Experimental section; Figure S1 and S2 in SI). The carbon fibers are covered by nanowires with a typical length of about 300 nm and diameters of 20~50 nm (Figure S1). These as-prepared TiO_2 nanowires were further annealed in air at 550 °C for 60 minutes (denoted as Air-TiO_2) in order to increase the crystallinity of TiO_2. From the SEM studies, there is no obvious morphological change in nanowire structure during the thermal treatment (Figure S3). The Air-TiO_2 was further annealed at temperature of 550 °C in hydrogen atmosphere for another 60 minutes (denoted as hydrogenated-TiO_2) to create the Ti^{3+}. Figure 1 shows the SEM image of the hydrogenated-TiO_2 and it can be observed that the nanowire structure still remain unchanged. Figure 1c shows the TEM images recorded from representative TiO_2 nanowire arrays. It can be obeserved that these nanowires are single crystals (Figure 1c inset down), which grows along the [002] axis. The upper of Figure 1c displays the HRTEM collected at the edge of the nanowires with lattice fringes of 0.14 and 0.32 nm (Figure 1d), which corresponds with the d-spacing of (002) and (111) planes of the rutile TiO_2 phase (JCPDF #: 65-0190).

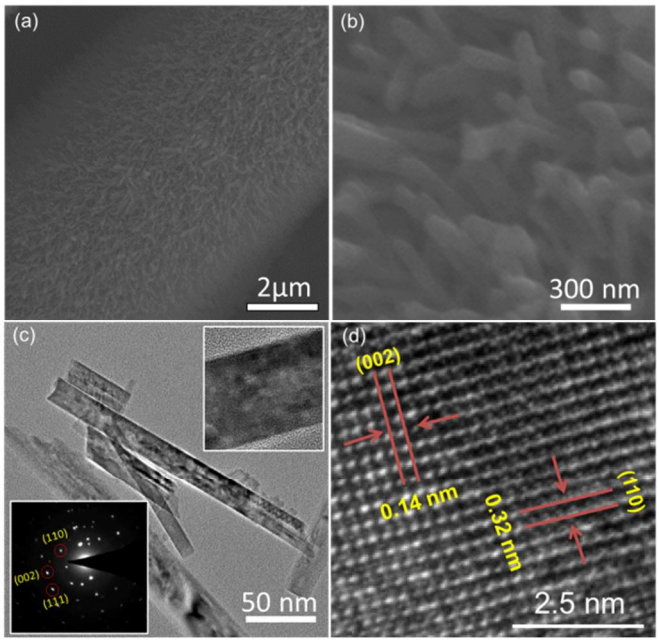

Figure 1. (a) SEM image of hydrogenated-TiO_2 nanowire arrays. (b) Magnified SEM image of nanowires. (c) TEM images of hydrogenated-TiO_2. Inset: HRTEM image (up) and SAED pattern (down). (d) Lattice-resolved image collected at the edge of the nanowire.

XRD spectra collected from Air-TiO_2 and hydrogenated-TiO_2 are shown in Figure 2a. Apart from the diffraction peaks originating from the carbon fiber substrates (circle symbol), the peaks collected from the Air-TiO_2 can be well indexed to the tetragonal TiO_2 (JCPDF #: 65-0190) (Figure 2a). There is no obvious shift in the diffraction peaks between Air-TiO_2 and the hydrogenated-TiO_2 samples. Furthermore, the Raman analysis shows that the characteristics Raman peaks of rutile TiO_2 shifted towards the low Raman shift and slightly broaden. Additionally, the peak intensity for the hydrogenated–TiO_2 sample decreases when compared with the air-TiO_2 sample (Figure 2b). Such the shift suggests the increased in the amount of oxygen vacancies in hydrogenated-TiO_2 sample. [26, 32]

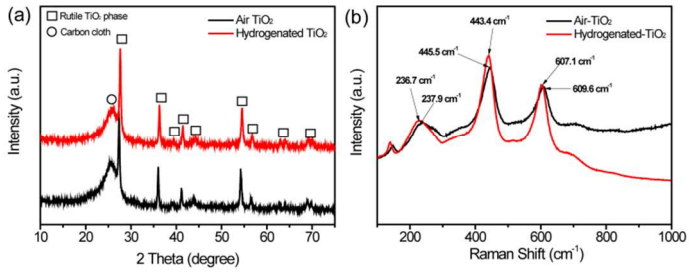

Figure 2. (a) XRD spectra of Air-TiO_2 and hydrogenated-TiO_2 samples. The diffraction peaks of rutile TiO_2 and carbon fiber are highlighted by square and circle symbols respectively. (b) Raman spectra of Air-TiO_2 and hydrogenated-TiO_2 samples.

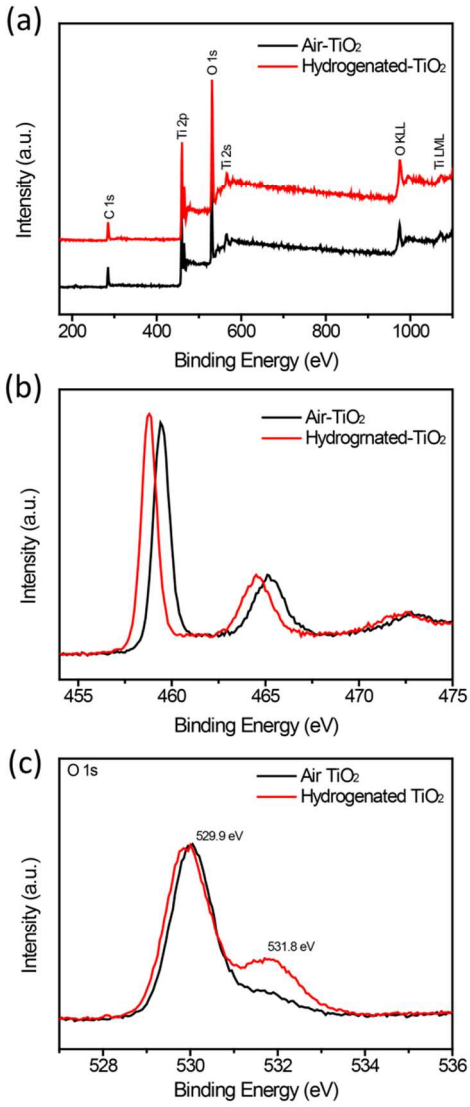

Figure 3. (a) XPS survey spectra of Air-TiO_2 and hydrogenated-TiO_2 samples. (b) Core level Ti 2p XPS spectra collected for Air-TiO_2 and hydrogenated-TiO_2 samples. (c) Core level O 1s XPS spectra collected for Air-TiO_2 and hydrogenated-TiO_2 samples.

X-ray photoelectron spectroscopy (XPS) studies were carried out to further investigate the hydrogenation effect on the chemical composition and oxidation state of TiO_2 nanowire arrays. Figure 3a displays the XPS survey spectra of the Air-TiO_2 and hydrogenated-TiO_2 samples. The intensity of the peaks increases after hydrogenation. Two broad peaks were centered at ~465.1 and~459.4 eV in the core level Ti 2p XPS spectra (Figure 3b). These two peaks correspond to the characteristic Ti $2p_{1/2}$ and Ti $2p_{3/2}$ peaks of the Ti^{4+} for the Air-TiO_2 sample. [26, 28] When compare with Air–TiO_2 sample, the hydrogenated-TiO_2 sample peaks shifted towards the negative binding energy at ~464.5 and ~458.8 eV, suggesting that the formation of the Ti^{3+} and resulting in oxygen vacancies. [33, 34] This result agrees well with the Raman analysis (Figure 2b). As shown in Figure 3c, the peak at 529.9 eV that observed for the Air–TiO_2 and hydrogenated-TiO_2 samples corresponds to the characteristic peak of Ti–O–Ti [27] Additional peak centered at 531.8 eV was observed for the hydrogenated-TiO_2 sample, which is attributed to Ti–OH. [28] This reveals that more functionalized hydroxyl group was formed on the surface of the hydrogenated-TiO_2 sample.

To study the electrochemical performance of the samples, electrochemical properties of the hydrogenated-TiO_2 and Air-TiO_2 samples were performed in a coin-type half-cell. Figure 4a and 4b show the 1st and 2nd discharge profiles of Air-TiO_2 and hydrogenated-TiO_2 sample at a current density of 1 C in the voltage range of 0.01 - 3 V. The hydrogenated-TiO_2 electrode achieved a first discharge capacity of 517 mAh g^{-1}, which is higher than the Air-TiO_2 (400 mAh g^{-1}) at the same current density and the theoretical capacity of TiO_2 at 335 mAh g^{-1} (Figure 4a). In Figure 4b, the discharge capacities of the two electrodes decrease as a result of the SEI layer, which is a common feature of LIB electrodes. [35-38] The 2nd discharge capacity of the Air-TiO_2 electrode was 296 mAh g^{-1}, which the coulombic efficiency was about 74%. However, the hydrogenated-TiO_2 electrode shows a higher coulombic efficiency of 84% with discharge capacity of 424 mAh g^{-1}. This suggests that the hydrogenated electrode is capable of reducing the SEI layer formation. Upon SEI layer formation, the discharge capacity of the hydrogenated-TiO_2 was higher than the theoretical capacity of the TiO_2 (335 mAh g^{-1}). This is due to the contribution of the carbon fiber when the electrode was discharged to a voltage of 0.01 V. The peak at the low voltage region (around 0.6 V) can be associated with the lithiation behavior of the carbon fiber. [17] The carbon fiber, which do not only function as a binder free substrate for the TiO_2 nanowires, but also contributed to increase in the discharge capacity of the electrodes. Moreover, the hydrogenated-TiO_2 electrode possesses better cyclic stability than the Air-TiO_2 electrode. As shown in Figure S4, the discharge capacity of the hydrogenated-TiO_2 electrode achieved 411 mAh g^{-1} at 1 C after 50 cycles with 80% capacity retention of its initial capacity, while the corresponding values for the Air-TiO_2 was 264 mAh g^{-1} (66% of its initial capacity).

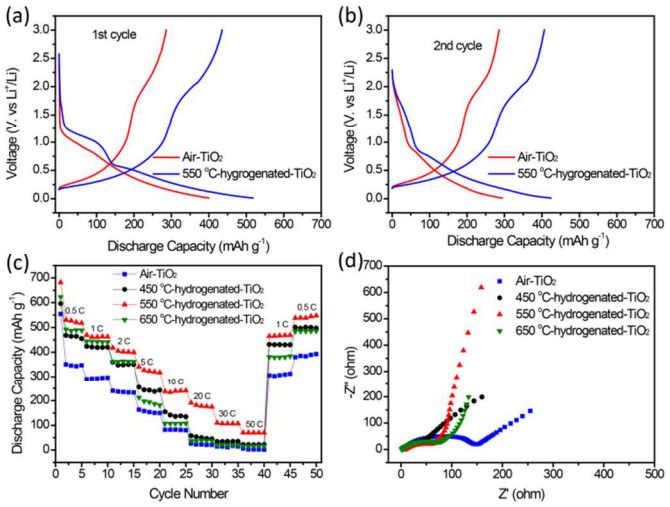

Figure 4. Electrochemical Properties of Air-TiO_2 and hydrogenated-TiO_2 electrodes. (a) First charge-discharge curves. (b) Second charge-discharge curves. (c) Rate capability profiles. (d) Nyquist plots.

It is important to sutdy the degree of hydrogenation on the electrochemical performance of the TiO_2 nanowires. At this stage, we annealed the Air-TiO_2 at 450 °C (450 °C-hydrogenated-TiO_2) and 650 °C (650 °C-hydrogenated-TiO_2). To study the effect of current density on the performance of Air-TiO_2 and hydrogenated-TiO_2 samples, we increased the current density gradually from 0.5 C to 50 C. As shown in Figure 4c, the discharge capacities of the

hydrogenated-TiO_2 samples were higher than the Air-TiO_2 at each current density. At a high current density of 50 C, the 550 ^oC-hydrogenated-TiO_2 sample was able to deliver a capacity of 70 mAh g^{-1}, which is about 47 times high than the Air-TiO_2 sample (1.5 mAh g^{-1}) and 3-4 times higher than the corresponding hydrogenated samples at 450 ^oC and 650 ^oC. With respect to temperature difference of the hydrogenated samples, it was observed that the discharge capacity of the 650 ^oC-hydrogenated-TiO_2 was higher than that of 450 ^oC-hydrogenated-TiO_2 at current density of 2 C and becomes lower when the current density increases. This suggests that the hydrogenation increases with increasing temperature. The discharge capacities of the 550 ^oC-hydrogenated-TiO_2 at each current density are higher than or comparable to the recently reported TiO_2 electrode materials [2, 11, 15] such as nitridated TiO_2 [39], TiO_2-B nanosheets [16], porous TiO_2-Carbon Nanofibers [40], multifunctional TiO_2–C/MnO_2 [1], TiO_2-Graphene-Carbon Nanotube [12] and hydrogenated TiO_2 nanotube arrays. [33] When the current density was decreased back to low current density of 0.5 and 1 C, unlike Air-TiO_2 that could not retain its initial capacity after subsequent cycling at higher current density, the hydrogenated-TiO_2 samples could retain their initial capacities. Such performance indicates the excellent rate capability of the hydrogenated-TiO_2 electrode. Hence, hydrogenated-TiO_2 exhibited higher lithium-ion storage capacity and better rate capability than the Air-TiO_2, which is due to improved storage kinetics as a result of the formation of Ti^{3+} (oxygen vacancies) via hydrogenation. Electrochemical impedance spectroscopy was used to study the electrochemical behaviors of Air-TiO_2 and hydrogenated-TiO_2 electrodes. Figure 4d and Figure S5 present the Nyquist plots and the equivalent circuit of Air-TiO_2 and the hydrogenated-TiO_2 electrodes. The semi-circle represents the charge-transfer resistance (R_{ct}) of the electrodes. As expected, the 550 ^oC-hydrogenated-TiO_2 electrode shows a much smaller R_{ct} value of 77.6 Ω than that of the Air-TiO_2 (153.2 Ω), showing the hydrogenated-TiO_2 possesses better electronic conductivity than that of Air-TiO_2. Also, the R_{ct} of the 550 ^oC-hydrogenated-TiO_2 is smaller than those of hydrogenated-TiO_2 annealed at 450 ^oC (99.7 Ω) and 650 ^oC (119.8.7 Ω). Warburg system dominates the impedance plot for a reversible electrochemical system. Increase in the slope of Warburg line suggests fast lithium insertion and extraction. [41, 42] Thus, the Warburg line of the hydrogenated-TiO_2, which displays a slope at an angle near 90^o, exhibits superior discharge capacity over Air-TiO_2 with a slope angle of about 45^o.

The long-term cycling performance of the hydrogenated-TiO_2 sample was also examined a current density of 10 C. Figure 5a shows the cyclic stability of the hydorgenated-TiO_2 at current density of 10 C for 500 cycles. The hydrogenated-TiO_2 displays a discharge capacity of 164 mAh g^{-1} after 500 cycles achieving capacity retention of 66% from its initial capacity (250 mAh g^{-1}at the 1st cycle). Such superior discharge capacity and excellent stability of the hydrogenated-TiO_2 could be attributed to the formation of the oxygen vacancies, which effectively enhanced lithium-ion storage capacity. The lithium storage mechanism of the Air-TiO_2 and hydrogenated-TiO_2 was compared using the cyclic voltammogram (CV) curves as shown in Figure 5b and 5c. In the first cycle, the peak shape of the hydrogenated-TiO_2 was sharper and intense than that of the Air-TiO_2 (Figure 5b). In the second cycle, the redox peak of Air-TiO_2 becomes broadened while the redox peak can still be maintained in the Hydrogenated TiO_2 (Figure 5c). This suggests that the hydrogenated sample have more effective lithium storage capacity that the Air-TiO_2. Also, the gap between redox peaks of the hydrogenated-TiO_2 was smaller than that of Air-TiO_2 demonstrating that the total resistance of the hydrogen-treated electrode is lower than that of the air-treated electrode, which was also confirmed by the EIS measurement (Figure 4d). Also, the peaks at the lower voltage region (0.6 V) correspond to the redox peaks of the carbon fiber, which is also in good agreement with the charge-discharge profiles in Figure 4a.

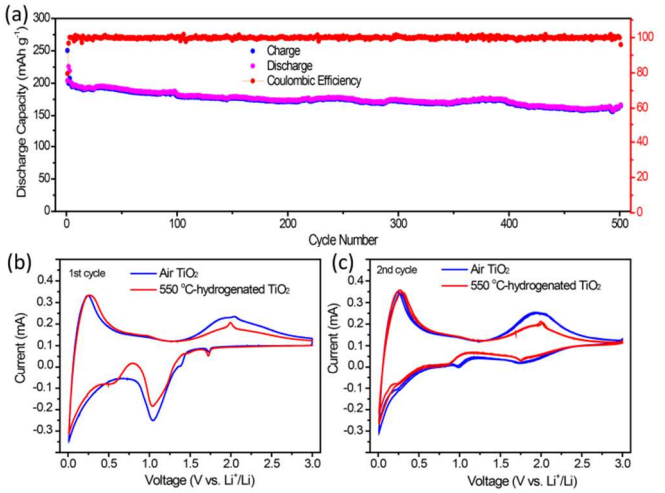

Figure 5. (a) Cycling performance of hydrogenated-TiO_2 at the rate of 10 C for 500 cycles. (b) First cycle and (c) second cycle cyclic voltammograms of Air-TiO_2 and hydrogenated-TiO_2.

Conclusion

In summary, flexible free-standing hydrogenated-TiO_2 has been fabricated via hydrothermal growth and hydrogen treatment. The flexible free-standing hydrogenated-TiO_2 ensures fast lithium storage due to Ti^{3+} (oxygen vacancies) formation. The flexible carbon fiber support allows facile access of ions and also provides the electrode with good conductivity and high mechanical flexibility. Hence, such flexible binder-free hydrogenated-TiO_2 electrode exhibits high reversible capacity of 517 mAh g^{-1} at 1 C, excellent rate capability as well as superior stability. This type of flexible binder-free electrodes could create great opportunity for the development of more flexible LIB electrodes.

Acknowledgements

We acknowledge the financial support of this work by the R-D-SBES-R—R & D in Sustainable Building Energy Systems and Retrofitting (NO: FP7-PEOPLE-2010-IRSES-269205).

Notes and references

[a] School of Chemistry and Chemical Engineering, GuangDong Pharmaceutical University, Guangzhou 510006, China
*Contact information for corresponding authors:
Email: liuyi915@126.com

Electronic Supplementary Information (ESI) available: Detailed experimental section. See DOI: 10.1039/c000000x/

1. J.-Y. Liao, D. Higgins, G. Lui, V. Chabot, X. Xiao and Z. Chen, *Nano Lett.*, 2013, **13**, 5467-5473.
2. Y. Luo, J. Luo, J. Jiang, W. Zhou, H. Yang, X. Qi, H. Zhang, H. J. Fan, D. Y. W. Yu, C. M. Li and T. Yu, *Energy Environ. Sci.*, 2012, **5**, 6559-6566.
3. M.-H. Ryu, K.-N. Jung, K.-H. Shin, K.-S. Han and S. Yoon, *J. Phys. Chem. C*, 2013, **117**, 8092-8098.

4. A. G. Dylla, G. Henkelman and K. J. Stevenson, *Acc. Chem. Res.*, 2013, **46**, 1104-1112.
5. S. Liu, H. Jia, L. Han, J. Wang, P. Gao, D. Xu, J. Yang and S. Che, *Adv. Mater.*, 2012, **24**, 3201-3204.
6. H. Han, T. Song, E.-K. Lee, A. Devadoss, Y. Jeon, J. Ha, Y.-C. Chung, Y.-M. Choi, Y.-G. Jung and U. Paik, *ACS Nano*, 2012, **6**, 8308-8315.
7. A. R. Armstrong, G. Armstrong, J. Canales, R. García and P. G. Bruce, *Adv. Mater.*, 2005, **17**, 862-865.
8. Y. Ren, Z. Liu, F. Pourpoint, A. R. Armstrong, C. P. Grey and P. G. Bruce, *Angew. Chem. Int. Ed.*, 2012, **124**, 2206-2209.
9. Y. Qiu, K. Yan, S. Yang, L. Jin, H. Deng and W. Li, *ACS Nano*, 2010, **4**, 6515-6526.
10. X. Zhang, P. Suresh Kumar, V. Aravindan, H. H. Liu, J. Sundaramurthy, S. G. Mhaisalkar, H. M. Duong, S. Ramakrishna and S. Madhavi, *J. Phys. Chem. C*, 2012, **116**, 14780-14788.
11. J. S. Chen, Z. Wang, X. C. Dong, P. Chen and X. W. D. Lou, *Nanoscale*, 2011, **3**, 2158-2161.
12. L. Shen, X. Zhang, H. Li, C. Yuan and G. Cao, *J. Phys. Chem. Lett.*, 2011, **2**, 3096-3101.
13. Z. Yang, G. Du, Z. Guo, X. Yu, Z. Chen, T. Guo and H. Liu, *J. Mater. Chem.*, 2011, **21**, 8591-8596.
14. Z. Yang, G. Du, Q. Meng, Z. Guo, X. Yu, Z. Chen, T. Guo and R. Zeng, *J. Mater. Chem.*, 2012, **22**, 5848-5854.
15. P. Zhang, J. Qiu, Z. Zheng, G. Liu, M. Ling, W. Martens, H. Wang, H. Zhao and S. Zhang, *Electrochimica Acta*, 2013, **104**, 41-47.
16. S. Liu, Z. Wang, C. Yu, H. B. Wu, G. Wang, Q. Dong, J. Qiu and A. Eychmüller, *Adv. Mater.*, 2013, **25**, 3462-3467.
17. M.-S. Balogun, M. Yu, C. Li, T. Zhai, Y. Liu, X. Lu and Y. Tong, *J. Mater. Chem. A*, 2014, DOI: 10.1039/C4TA00987H.
18. T. Hu, X. Sun, H. Sun, M. Yu, F. Lu, C. Liu and J. Lian, *Carbon*, 2013, **51**, 322-326.
19. B. Zhao, R. Cai, S. Jiang, Y. Sha and Z. Shao, *Electrochim. Acta*, 2012, **85**, 636-643.
20. F. Cheng, T. Zhang, Y. Zhang, J. Du, X. Han and J. Chen, *Angew. Chem. Int. Ed.*, 2013, **52**, 2474-2477.
21. T. Zhai, S. Xie, M. Yu, P. Fang, C. Liang, X. Lu and Y. Tong, *Nano Energy*, 2014, **8**, 255-263.
22. X. Han, F. Cheng, T. Zhang, J. Yang, Y. Hu and J. Chen, *Adv. Mater.*, 2014, **26**, 2047-2051.
23. X. Lu, Y. Zeng, M. Yu, T. Zhai, C. Liang, S. Xie, M. S. Balogun and Y. Tong, *Adv. Mater.*, 2014, **26**, 3148-3155.
24. M. Li, Y. Hu, S. Xie, Y. Huang, Y. Tong and X. Lu, *Chem. Commun.*, 2014, **50**, 4341-4343.
25. S. Xie, T. Zhai, W. Li, M. Yu, C. Liang, J. Gan, X. Lu and Y. Tong, *Green Chem.*, 2013, **15**, 2434-2440
26. X. Lu, G. Wang, T. Zhai, M. Yu, J. Gan, Y. Tong and Y. Li, *Nano Lett.*, 2012, **12**, 1690-1696.
27. X. Lu, M. Yu, G. Wang, T. Zhai, S. Xie, Y. Ling, Y. Tong and Y. Li, *Adv. Mater.*, 2013, **25**, 267-272.
28. G. Wang, H. Wang, Y. Ling, Y. Tang, X. Yang, R. C. Fitzmorris, C. Wang, J. Z. Zhang and Y. Li, *Nano Lett.*, 2011, **11**, 3026-3033.
29. C. Xu, Y. Song, L. Lu, C. Cheng, D. Liu, X. Fang, X. Chen, X. Zhu and D. Li, *Nanoscale Res. Lett.*, 2013, **8**, 1-7.
30. T. Leshuk, R. Parviz, P. Everett, H. Krishnakumar, R. A. Varin and F. Gu, *ACS Appl. Mater. Interfaces*, 2013, **5**, 1892-1895.
31. P. Yang, X. Xiao, Y. Li, Y. Ding, P. Qiang, X. Tan, W. Mai, Z. Lin, W. Wu and T. Li, *ACS Nano*, 2013, **7**, 2617-2626.
32. G. Wang, Y. Ling, H. Wang, X. Yang, C. Wang, J. Z. Zhang and Y. Li, *Energy Environ. Sci.* 2012, **5**, 6180-6187.
33. Z. Lu, C. T. Yip, L. Wang, H. Huang and L. Zhou, *ChemPlusChem*, 2012, **77**, 991-1000.
34. L. Shen, E. Uchaker, X. Zhang and G. Cao, *Adv. Mater.*, 2012, **24**, 6502-6506.
35. H. Huang, Y. Liu, J. Wang, M. Gao, X. Peng and Z. Ye, *Nanoscale*, 2013, **5**, 1785-1788.
36. J. Deng, Z. Lu, I. Belharouak, K. Amine and C. Y. Chung, *J. Power Sources*, 2009, **193**, 816-821.
37. C. Liang, T. Zhai, W. Wang, J. Chen, W. Zhao, X. Lu and Y. Tong, *J. Mater. Chem. A*, 2014, **2**, 7214-7220.
38. Y. Qiu, K. Yan and S. Yang, *Chem. Commun.*, 2010, **46**, 8359-8361.
39. H. Han, T. Song, J.-Y. Bae, L. F. Nazar, H. Kim and U. Paik, *Energy Environ. Sci.*, 2011, **4**, 4532-4536.
40. X. Li, Y.-m. Chen, L. Zhou, Y.-W. Mai and H. Huang, *J. Mater. Chem. A*, 2014, **2**, 3875-3880.
41. B.-Y. Chang and S.-M. Park, *Ann. Rev. Anal. Chem.*, 2010, **3**, 207-229.
42. D. D. Macdonald, *Electrochim. Acta*, 2006, **51**, 1376-1388.

Graphical Abstract